## PAPER

Check for updates

Cite this: RSC Adv., 2023, 13, 22281

# Improvement of optical properties of AISI 304 as a solar absorber using a pulsed fiber laser†

Narin Chomcharoen, [ID] [a] Tanyakorn Muangnapoh,[b] Bhawat Traipattanakul[c] and Krissada Surawathanawises*[a]

Solar energy is an environmentally friendly and inexhaustible natural resource. It can be converted into thermal energy by using concentrated solar power (CSP) methods. One of the key components of CSP is a solar absorber, which absorbs concentrated solar radiation and converts it into heat. Recently, there have been many studies on enhancing the solar-to-thermal conversion efficiency of solar absorbers. In this work, a pulsed fiber laser was used to modify the surface of AISI 304 stainless steel as a solar absorbing material. By varying the energy density, surface roughness and oxide films can be formed, which affect the solar absorptance and thermal emittance of the substrate. The surface characteristics and corresponding optical properties were investigated. The surface roughness was measured to be in the range of 9–158 nm. Due to heat generated during engraving, metal surface oxidation occurs on the AISI 304 substrate, resulting in different values of solar absorptance and thermal emittance. Compared with the unmodified surface, the modified AISI 304 surfaces resulted in solar absorptance ranging from 58.57% to 91.78%, and the thermal emittance ranged from 10.56% to 32.90%. Consequently, the solar-to-thermal conversion efficiency was improved from 50.09% to 81.69%, and the technique can be used for solar absorbing applications.

## Introduction

To generate electricity, conventional resources such as fossil fuels or coal have been used. However, they have adverse effects on the environment, so the use of alternative resources has been explored. Concentrated solar power (CSP) technology can convert solar irradiance into thermal energy, which can be used for electricity generation.[1] In general, solar radiation is reflected by a reflector and concentrated onto a solar absorber to generate heat. The heat is then transferred to a heat-transfer fluid (HTF), which is later used for electricity generation with a conventional steam turbine.[2] The operation of CSP is demonstrated in Fig. 1(a). One of the key elements to control solar-to-thermal conversion efficiency is the optical properties of the solar selective absorber (SSA) which deposited and enveloped the absorber tube as shown in Fig. 1(b). The quality of the solar selective absorber layer also controls achieve high solar absorptance ($\alpha_s$) and low thermal emittance ($\varepsilon_t$) in order to obtain the best conversion efficiency.[3]

There are many ways to obtain spectrally selective solar absorbers by surface modification, such as surface texturing,[4] creating surface roughness,[5] intrinsic structure or nano-structure formation,[6] cermet coating[7,8] and multilayer absorber coating.[9] The creation of an oxide layer as an intrinsic structure and surface roughness is quite simple and produces good conditions for high solar absorptance and low thermal emittance. It is well-known that cermet-based is the most recent widely used as solar selective absorbers, which exhibit outstanding in spectral selectivity. The cermet-based absorber as selective surfaces have high solar absorptance at 0.96 and low thermal emittance at 0.09, which deposited on stainless steel surface under sputtering technique.

An oxide layer and surface roughness can be created with two types of atmospheric systems: vacuum-based and ambient-based systems. Sputtering[10] and electron evaporation are vacuum-based methods, and these high-cost processes use high amount of energy to create the oxide layer and surface roughness. Khelifa et al.[9] used electron beam evaporation to create multilayer absorbers based on $Cr_2O_3/Cr/Cr_2O_3$, which could improve the optical properties.

Sintering[11] and laser treatment[12–15] are ambient-based methods, and these low-cost processes can easily create the oxide layer and surface roughness. Laser treatment uses low energy and takes a short time for processing, while sintering operates at a high temperature and a longer time for processing. Wu et al.[11] created a solar absorber on AISI 304 by sintering, and

*aDepartment of Materials Engineering, Faculty of Engineering, Kasetsart University, Bangkok 10900, Thailand. E-mail: fengksds@ku.ac.th*

*bNational Nanotechnology Center (NANOTEC), National Science and Technology Development Agency (NSTDA), Pathum Thani 12120, Thailand*

*cSchool of Manufacturing Systems and Mechanical Engineering, Sirindhorn International Institute of Technology, Thammasat University, Thailand*

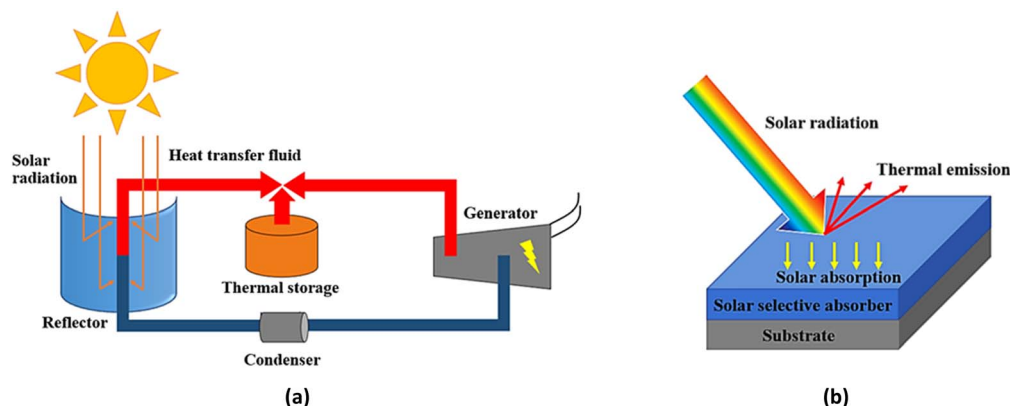† Electronic supplementary information (ESI) available. See DOI: https://doi.org/10.1039/d3ra03873d

**Fig. 1** Parabolic-trough solar concentrated power technology (a) schematic operation of parabolic-trough solar concentrated power (b) optical reaction mechanism on solar selective absorber which deposited on metal substrate.

a thick $Fe_2O_3$ oxide film layer was formed on the surface with roughness of 114.3 nm. As a result, the optical properties were improved. Jalil *et al.*[16] used femtosecond laser treatment to create a solar absorber with a variety of metals (copper, aluminum, steel, and tungsten). They controlled the scanning speed and frequency to activate the absorption due to plasmonic resonance of the oxide particles on the surface, and tungsten had the highest solar absorptance of 92% and the lowest thermal emittance of 18%.

In this research, AISI 304 was used as a solar absorbing material. Its surface was modified with a pulsed fiber laser to create an oxide layer for intrinsic structure formation[17] and roughness on the substrate.[18] Most current commercial technology enhances the photo-thermal conversion by fabricating the solar selective absorber under vacuum based conditions, such as sputtering technique. To compare with the pulsed fiber laser in this paper, this technique is under atmospheric conditions which make it easy to apply on an industrial scale. The pulsed fiber laser helps in growing intrinsic absorbers with rapid processing, which is easier, lower in energy and cost-effective. Moreover, there is no need for target materials as a solar selective absorber. These factors can affect the solar absorptance and thermal emittance of the substrate.[19] This process is scalable for commercial applications by utilizing a laser array for large surface modification, which also facilitates higher moving speeds, resulting in shorter completion times.[20] The microstructures and optical properties of specimens were investigated, and the solar-to-thermal conversion efficiency was evaluated.[21]

## Experimental

### Materials and methods

AISI 304 stainless steel sheets (1 inch × 1 inch and 1.0 mm thick) were cleaned with isopropyl alcohol by ultrasonic vibration for 5 minutes. Subsequently, the surfaces were treated with a pulsed fiber laser with a wavelength of 1064 nm in air, using an energy density ranging from 0.00 to 6.61 kJ inch$^{-2}$ to promote roughness and oxidation. The pulse diameter was 50 µm, the pulse frequency was 20 kHz, and the scanning speed was 200 mm min$^{-1}$. The laser spacing from center to center was maintained at 10 µm. The laser was operated in line scanning mode.[22] The energy density can be calculated from the following equation:[23]

$$\text{Energy density} = \frac{P(w) \times t(s)}{A(\text{inch}^2)} \quad (1)$$

where $P$ is the laser power in watts, $t$ is the exposure time in seconds counted from the onset of the pulse, and $A$ is the surface area of the treatment in inch$^2$. The energy density of all specimens is shown in Table 1.

### Characterization

The surface roughness was investigated by confocal microscopy, and the surface morphology was characterized by scanning electron microscopy (SEM; Hitachi SU-8230). The surface elements were characterized by energy-dispersive X-ray spectroscopy (EDS; Oxford Instruments) and an electron probe microanalyzer (Shimadzu EPMA-8050G). The oxide formation was studied by X-ray diffractometer (XRD; Bruker/D8 Advance) with $2\theta$ ranging from 20° to 90°. The optical properties were measured for the solar absorptance ($\alpha_s$) using spectrophotometry (Agilent technologies, Cary 5000 UV-Vis-NIR), and the solar absorptance was computed as follows:

$$\alpha_s = \frac{\int_{\lambda_1}^{\lambda_2} I_s(\lambda)(1 - R(\lambda))\mathrm{d}\lambda}{\int_{\lambda_1}^{\lambda_2} I_s(\lambda)\mathrm{d}\lambda} \quad (2)$$

where $I_s(\lambda)$ is the solar spectral radiation of air mass 1.5 from the ASTM G173 standard. $R(\lambda)$ is the measured reflectance at a specific wavelength $\lambda$ (wavelength interval $\lambda_1$ to $\lambda_2$ = 0.3 to 2.5 µm).[7] The thermal emittance ($\varepsilon_t$) was tested at 120 °C using an emissometer (Devices & Services Company, Model AE-ADI). Solar to thermal conversion efficiency was calculated from the eqn (3) as follow:

$$\text{Conversion efficiency} = (1 - \varepsilon_t) \times \alpha_s \quad (3)$$

**Table 1** Calculated energy densities of the laser

| Specimen | A | B | C | D | E | F | G | H | I | J |
|---|---|---|---|---|---|---|---|---|---|---|
| Energy density (kJ inch$^{-2}$) | 0.00 | 1.37 | 1.71 | 2.05 | 2.39 | 2.74 | 3.08 | 3.42 | 4.79 | 6.16 |

# Results and discussion

## Surface appearance

Fig. 2 shows the different surface appearances of the specimens after being treated with the pulsed fiber laser. Compared to unmodified specimen A, specimens B and C exhibited a slightly brighter surface, while specimen D appeared more yellowish. Specimen E had a dark blue surface, while the color of specimens F to H gradually faded out. Specimens I and J had a darker surface due to the higher laser power. The differences in surface appearance were attributed to the roughness and oxide formation during laser engraving.[24–26] The specimens also showed horizontal lines, which were caused by the line-scanning laser.

## Roughness analysis

The surface roughness ($R_a$) at different power was measured, and the result is presented in Fig. 3. From specimen A to C, the roughness decreased from 47 to 9 nm due to the surface treatment by the pulsed fiber laser, which smoothened the surface. Then, the roughness slightly increased from 9 to 27 nm from specimen C to H. This could have occurred because of metal oxide formation on the surface. From specimen I and J, the roughness significantly increased from 27 to 158 nm. Since heat accumulated at high laser power, the oxide layer could grow much faster and result in a rougher surface.[27,28] The height images presenting the roughness are shown in ESI.†

## Surface morphology and elemental analysis

The surface morphology of specimens was investigated by SEM, which showed that higher energy density created different surface structures, as shown in Fig. 4. Compared with non-laser treated specimen A (Fig. 4(a)), nano-sized particles were formed on the surfaces of specimen B to E. Accordingly, at higher laser

energies, more particles were formed and uniformly distributed over the surfaces (Fig. 4(b)). However, specimen F to H presented a combination of nano-sized particles and circle islands formed non-uniformly over the surfaces (Fig. 4(c)). Such the structure could contribute to a rougher surface. Formation of highly porous structure on specimen I and J was observed after they were modified with high laser energies. As a result, it could greatly increase the surface roughness (Fig. 4(d)).

The microstructural transformation of specimen B to J was expected to be a result of metal oxide formation generated from the laser treatment.[29,30] The elemental analysis showed that oxygen content was increased on the specimens treated with higher energy density, as shown in Fig. 5. The results indicated that surface oxidation occurred during the laser engraving.[31]

In addition, the XRD results showed that the non-modified stainless steel mainly consisted of α-Fe and γ-Fe phases. However, the constituent phases changed when the surface was modified by the pulsed fiber laser. The diffraction peaks in Fig. 6 presents $Cr_2O_3$ and $Fe_2O_3$ phases on the specimens treated with laser, which agreed well with a report by Cui *et al.*[32]

Although the metal oxides found on surfaces were characterized, the nano-sized particles and circle islands found on specimens (Fig. 4) were further investigated. Specimen E and G were studied using elemental mapping. Consequently, the results revealed different elemental concentrations of oxygen (O), chromium (Cr), and iron (Fe), over the surfaces as seen in Fig. 7. Specimen E, which consisted of nano-sized particles, presented uniform elemental concentrations of O, Cr, and Fe for entire surface (Fig. 7(a1)–(a4)). In contrast, there was a combination of nano-sized particles and large circle islands in specimen G observed in the diagonal band in Fig. 7(b1). From elemental mapping analysis (Fig. 7(b2)–(b4)), the circle islands were rich in Fe and O that could form an iron oxide while, within the band, the surrounded nano-sized particles were rich
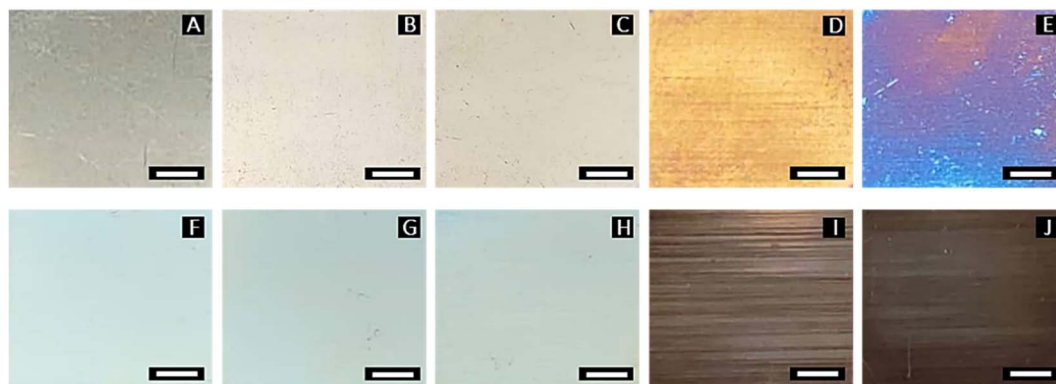


**Fig. 2** Surface appearance of AISI 304 specimens treated by pulsed fiber laser with different energy densities (A = 0.00, B = 1.37, C = 1.71, D = 2.05, E = 2.39, F = 2.74, G = 3.08, H = 3.42, I = 4.79, and J = 6.16 kJ inch$^{-2}$) as shown in Table 1 (scale bars are 5.0 mm).
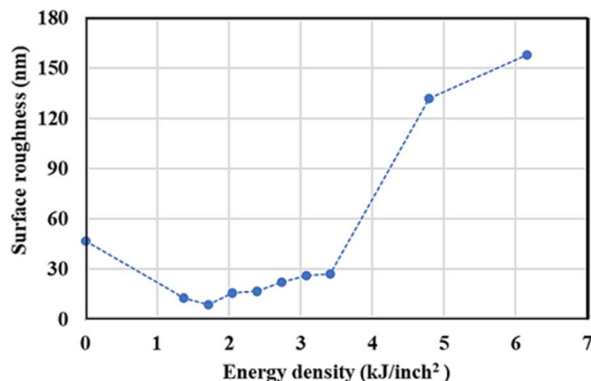
**Fig. 3** Surface roughness of AISI 304 stainless steel before and after modification by the pulsed fiber laser method with energy density between 0.00 and 6.16 kJ inch$^{-2}$ (specimen A to J).
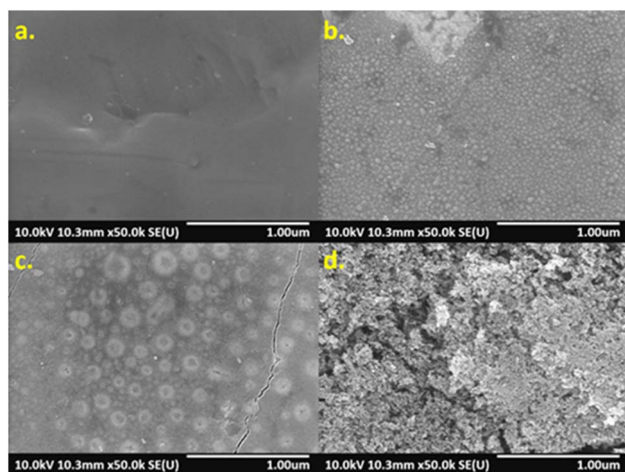


**Fig. 4** SEM images of AISI 304 surfaces. (a) specimen A, (b) specimen E, (c) specimen G, and (d) specimen J.



**Fig. 5** EDS of AISI 304 stainless steel before and after modification by the pulsed fiber laser method from specimen A, specimen E, specimen G, and specimen J.



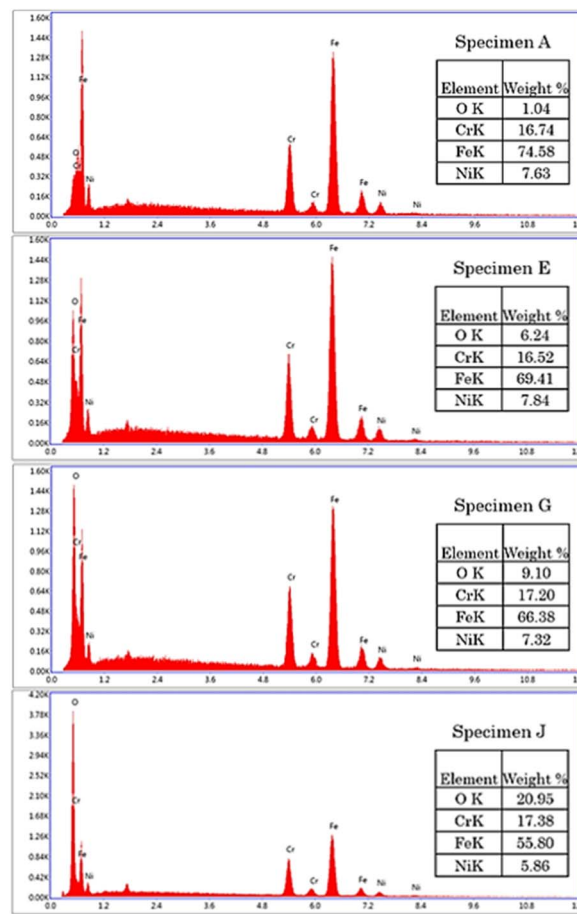**Fig. 6** XRD patterns of AISI 304 stainless steel before and after modification by the pulsed fiber laser method from specimen A, specimen E, specimen G, and specimen J.

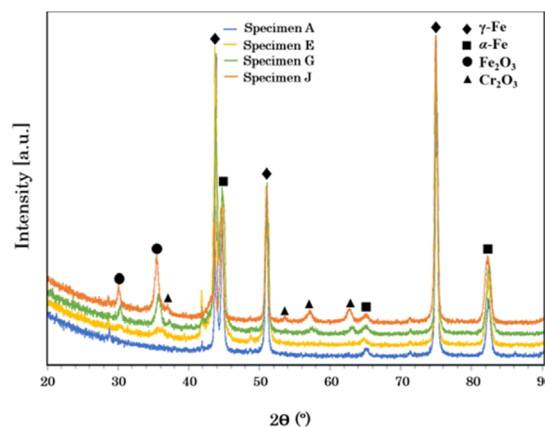in Cr and O that could form a chromium oxide. The difference in roughness and metal oxides on the surfaces treated by laser could lead to an improvement of the optical properties.[33–36]

### Optical property analysis

The non-modified and modified AISI 304 specimens were tested for $\alpha_s$ and $\varepsilon_t$, and the results are presented in Fig. 8. Initially, $\alpha_s$ of non-modified specimen A was 58.57% and was then improved up to 91.78% on specimen E. This improvement may be a result of the extended growth of $Cr_2O_3$ particles, which significantly influence the solar absorptance.[37] This influence is due to the regular distribution and plasmonic resonance of the oxide particles on the surface,[38,39] which originates from the resonance of collective conduction electrons with incident electromagnetic radiations. Moreover, small and uniform-sized nanoparticles with a narrow size distribution gives a sharp absorbance, whereas nanoparticles with a wide size distribution or any kind of aggregation show broad absorbance.[40] Next, $\alpha_s$ was reduced and remained around 78.47% from specimen F to

H. It was observed that, at higher laser energy, $Fe_2O_3$ could form on the surface while $Cr_2O_3$ particles were reduced and became non-uniformly distributed. In fact, the solar absorptance of $Fe_2O_3$ is lower compared with that of $Cr_2O_3$, as reported by
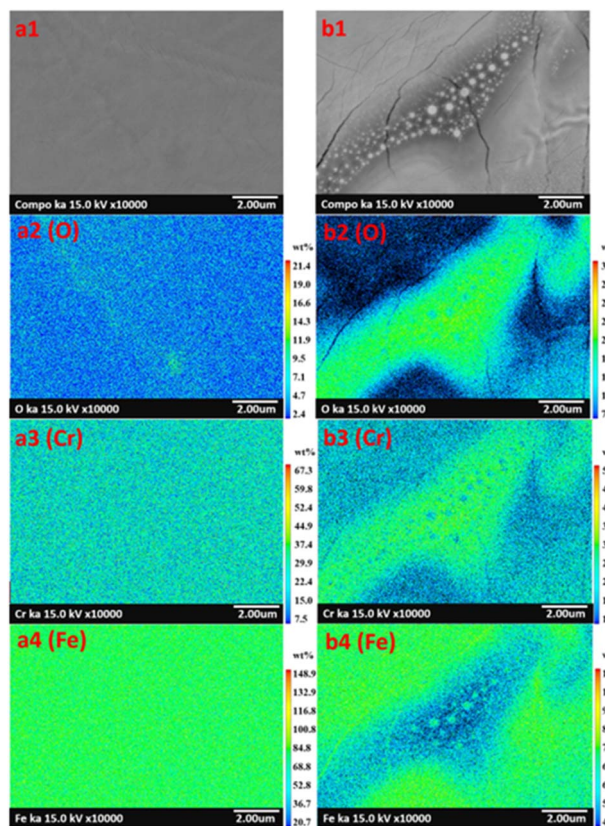
Fig. 7 Elemental image classification with color of modified AISI 304 surfaces presenting oxygen (O), chromium (Cr), and iron (Fe) in specimen E (image a1–a4), and in specimen G (image b1–b4).
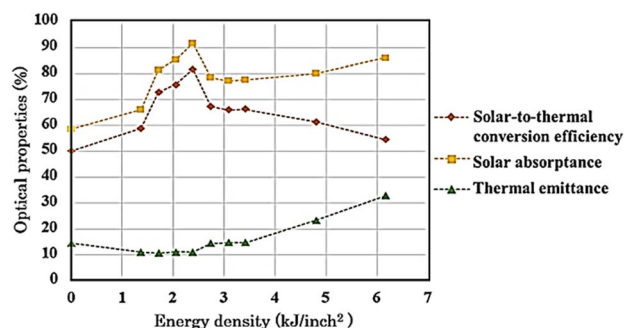


Fig. 8 Optical properties and solar-to-thermal conversion efficiency of AISI 304 stainless steel before and after modification by the pulsed fiber laser method with energy density of 0.00 to 6.16 kJ inch$^{-2}$.

Thakur and Yadav.[41] Then, $\alpha_s$ slightly increased again up to 86.14% from specimen H to J, and a porous $Fe_2O_3$ structure with high roughness was introduced. In general, when the roughness increases, the solar absorptance and thermal emittance also increase.[42,43] However, Bergström et al.[44] reported that if the surface roughness is below 150 nm, it may not affect the solar absorptance. Thus, the increase in $\alpha_s$ of specimen I and J could be from thicker $Fe_2O_3$ formation. The spectral reflectance data of modified specimens are presented in ESI.†

From Fig. 8, $\varepsilon_t$ decreased initially from 14.46% to 10.56% for specimen A to C, respectively. Afterwards, $\varepsilon_t$ remained relatively low and tended to increase from 11.13% to 32.90% for specimen D to J, respectively. The surface roughness and metal oxide formation were considered for the corresponding change in $\varepsilon_t$. Voinea et al.[45] reported that surface roughness could affect the thermal emittance proportionally. In this case, the resulting roughness (Fig. 3) had influenced the thermal emittance similarly. In addition, metal oxides also affect $\varepsilon_t$. Chromium oxide has a lower $\varepsilon_t$ compared to that of iron oxide.[41] Consequently, specimen D and E still kept $\varepsilon_t$ relatively low even though the roughness increased. Then, the solar-to-thermal conversion efficiency was calculated from $\alpha_s$ and $\varepsilon_t$, presented in Fig. 8. Overall, the efficiency was initially enhanced from 50.09% up to 81.69% for specimen A to E, respectively. After that, from specimen F to J, the higher energy density caused both $\alpha_s$ and $\varepsilon_t$ to increase. Nonetheless, $\alpha_s$ increased at a lower ratio. As a result, the efficiency decreased from 81.69% to 54.37%.

## Conclusions

This study presents the surface modification of AISI 304 stainless steel using a pulsed fiber laser. By varying the energy density, surface roughness and oxide formations were introduced, which can affect the optical properties. Initially, the surface roughness was found to be mostly lower than 150 nm, which had an insignificant effect on the solar absorptance. Based on the microstructural and elemental analyses, nano sized $Cr_2O_3$ particles and $Fe_2O_3$ islands were formed disparately depending on the laser power. At low power, $Cr_2O_3$ particles were dominant, and the solar absorptance of 91.78% was achieved. Although $Fe_2O_3$ became dominant at higher power, it yielded slightly lower solar absorptance up to 78.47%. The resulting oxide formation clearly enhanced the solar absorptance. Thermal emittance was also measured and found to be mainly affected by surface roughness. Rougher surfaces increased thermal emittance in a range of 9–158 nm in this study. Finally, with the pulsed fiber laser modification on AISI 304, a solar-to-thermal conversion efficiency from 50.09% up to 81.69% could be achieved. The process was quick and effective, and therefore has great potential for use in solar-absorbing applications in CSP technology.

## Conflicts of interest

There are no conflicts to declare.

## Acknowledgements

## References

1 L. A. Weinstein, J. Loomis, B. Bhatia, D. M. Bierman, E. N. Wang and G. Chen, *Chem. Rev.*, 2015, **115**, 12797–12838.

2  Q. Chen, Y. Wang, J. Zhang and Z. Wang, *Energies*, 2020, **13**, 1988.

3  M. Bello, S. Subramani and M. M. Bin Mohd Rashid, *Results Phys.*, 2020, **19**, 103582.

4  C. Niu, T. Zhu and Y. Lv, *Int. J. Photoenergy*, 2019, **2019**, 1476217.

5  E. S. P. Leong, Y. J. Liu, B. Wang and J. Teng, *ACS Appl. Mater. Interfaces*, 2011, **3**, 1148–1153.

6  X.-H. Gao, Z.-M. Guo, Q.-F. Geng, P.-J. Ma, A.-Q. Wang and G. Liu, *Sol. Energy Mater. Sol. Cells*, 2017, **163**, 91–97.

7  Z. Li, J. Zhao and L. Ren, *Sol. Energy Mater. Sol. Cells*, 2012, **105**, 90–95.

8  J. Yang, H. Shen, Z. Yang and K. Gao, *ACS Appl. Mater. Interfaces*, 2021, **13**, 14587–14598.

9  A. B. Khelifa, S. Khamlich, Z. Y. Nuru, A. Mebrahtu, M. Balgouthi, A. A. Guizani, W. Dimassi and M. Maaza, *J. Alloys Compd.*, 2018, **734**, 204–209.

10  A. Dan, K. Chattopadhyay, H. C. Barshilia and B. Basu, *Thin Solid Films*, 2016, **620**, 17–22.

11  S. Wu, C.-H. Cheng, Y.-J. Hsiao, R.-C. Juang and W.-F. Wen, *Renewable Sustainable Energy Rev.*, 2016, **58**, 574–580.

12  X. Pang, Q. Wei, J. Zhou and H. Ma, *Materials*, 2018, **11**, 1037.

13  L. Wang, K. Yin, Q. Deng, Q. Huang, J. He and J.-A. Duan, *Adv. Sci.*, 2022, **9**, 2204891.

14  Y. He, L. Wang, T. Wu, Z. Wu, Y. Chen and K. Yin, *Nanoscale*, 2022, **14**, 9392–9400.

15  K. Yin, Z. Wu, J. Wu, Z. Zhu, F. Zhang and J.-A. Duan, *Appl. Phys. Lett.*, 2021, **118**, 211905.

16  S. A. Jalil, B. Lai, M. ElKabbash, J. Zhang, E. M. Garcell, S. Singh and C. Guo, *Light: Sci. Appl.*, 2020, **9**, 14.

17  X. Ma, X. Nie, J. Zhao, P. Shrotriya, Y. Zhang, Y. Cui and J. Wang, *Opt. Laser Technol.*, 2020, **126**, 106104.

18  K. Mroczkowska, A. Antonczak, B. Szubzda, M. Wójcik, B. Stepak, P. Szymczyk-Ziółkowska, M. Trzcinski, M. Ozimek and K. Abramski, *J. Laser Appl.*, 2016, **28**, 032009.

19  C. Y. Cui, X. G. Cui, Y. K. Zhang, K. Y. Luo, Q. Zhao, J. D. Hu, Z. Liu and Y. M. Wang, *Appl. Surf. Sci.*, 2010, **256**, 6782–6786.

20  F. Ihsan, L. Daniault, S. Bellanger, M. Veinhard, J. Bourderionnet, C. Larat, E. Lallier, E. Durand, A. Brignon and J. C. Chanteloup, *Opt. Express*, 2020, **28**, 20152–20161.

21  H. Kügler and F. Vollertsen, *J. Manuf. Mater. Process.*, 2018, **2**, 84.

22  M. Radmanesh and A. Kiani, *Mater. Sci. Appl.*, 2015, **6**, 634.

23  T. Mileto and F. Azambuja, *RGO, Rev. Gaucha Odontol.*, 2017, **65**, 13–19.

24  Y. Lu, X. Shi, Z. Huang, T. Li, M. Zhang, J. Czajkowski, T. Fabritius, M. Huttula and W. Cao, *Sci. Rep.*, 2017, 7, 7092.

25  J.-T. Wang, C.-I. Weng, J.-G. Chang and C.-C. Hwang, *J. Appl. Phys.*, 2000, **87**, 3245–3253.

26  Y. Tamamura and G. Miyaji, *Opt. Mater. Express*, 2019, **9**, 2902–2909.

27  M. G. S. Ferreira, N. E. Hakiki, G. Goodlet, S. Faty, A. M. P. Simões and M. Da Cunha Belo, *Electrochim. Acta*, 2001, **46**, 3767–3776.

28  G. Schnell, U. Duenow and H. Seitz, *Materials*, 2020, **13**, 969.

29  V. P. Veiko, G. Odintsova, E. Ageev, J. Karlagina, A. Loginov, A. Skuratova and E. Gorbunova, *Opt. Express*, 2014, **22**, 24342–24347.

30  J.-M. Guay, A. Calà Lesina, G. Côté, M. Charron, D. Poitras, L. Ramunno, P. Berini and A. Weck, *Nat. Commun.*, 2017, **8**, 16095.

31  S. K. Lawrence, D. P. Adams, D. F. Bahr and N. R. Moody, *Surf. Coat. Technol.*, 2016, **285**, 87–97.

32  C. Y. Cui, X. G. Cui, X. D. Ren, M. J. Qi, J. D. Hu and Y. M. Wang, *Appl. Surf. Sci.*, 2014, **305**, 817–824.

33  P. Gupta and M. Ramrakhiani, *Open Nanosci. J.*, 2009, **3**, 15–19.

34  P. Bonin, M. Gelin and A. Bugaiska, *Memory Cognition*, 2013, **42**, 370–382.

35  C. Garfinkel, I. White, E. Gerber, M. Jucker and M. Erez, *J. Clim.*, 2020, **33**, 5611–5633.

36  H.-B. Fu and J.-N. Yao, *J. Am. Chem. Soc.*, 2001, **123**, 1434–1439.

37  A. B. Khelifa, A. Soum-Glaude, S. Khamlich, H. Glénat, M. Balghouthi, A. A. Guizani, M. Maaza and W. Dimassi, *J. Alloys Compd.*, 2019, **783**, 533–544.

38  X. Ding, C. H. Liow, M. Zhang, R. Huang, C. Li, H. Shen, M. Liu, Y. Zou, N. Gao, Z. Zhang, Y. Li, Q. Wang, S. Li and J. Jiang, *J. Am. Chem. Soc.*, 2014, **136**, 15684–15693.

39  M. Roy, S. Ghosh and M. K. Naskar, *Mater. Chem. Phys.*, 2015, **159**, 101–106.

40  J. Singh, V. Jaswal, A. Arora, M. Kinger and V. Gupta, *Orient. J. Chem.*, 2014, **30**, 559–566.

41  P. Thakur, A. Thakur and K. Yadav, *Springer Proc. Phys.*, 2017, **178**, 145–155.

42  E. Sani, L. Mercatelli, M. Meucci, L. Zoli and D. Sciti, *Sci. Rep.*, 2017, **7**, 718.

43  D. Bergstrom, J. Powell and A. Kaplan, *J. Appl. Phys.*, 2008, **103**, 103515.

44  D. Bergstrom, J. Powell and A. Kaplan, *J. Appl. Phys.*, 2007, **101**, 113504.

45  M. Voinea, M. Dudita, C. Cristina and A. Duta, *J. Optoelectron. Adv. Mater.*, 2009, **1**, 1130.